Paper IV

Ilker Fer, Miles G. McPhee and Anders Sirevaag

Conditional statistics of the Reynolds stress in the under-ice boundary layer

Conditional statistics of the Reynolds stress in the under-ice boundary layer

Ilker Fer, Miles G. McPhee and Anders Sirevaag

Abstract

Velocity fluctuations at 1 m and 5 m below pack-ice drifting at an average speed of 15 cm s^{-1} are analyzed to describe the conditional statistics of Reynolds stress in the under-ice boundary layer under melting conditions. The fractional contributions to the Reynolds stress show that ejection and sweep events dominate over interaction events. The sweeps are found to be more intense close to the boundary where the third and higher order moments are most pronounced. Third order cumulant expansions are found to describe the conditional Reynolds stress statistics reasonably well. Existing models for the turbulent kinetic energy transport term using cumulant expansion methods capture the effect of observed increase in the friction velocity with depth.

Introduction

In turbulent boundary layers, coherent structures with large flux events have been proposed to explain the "bursting" phenomena responsible for most turbulence production, hence mixing, through two types of organized eddy motions recognized as "ejections" and "sweeps" [see *Cantwell*, 1981; *Robinson*, 1991, for reviews]. These events are traditionally detected by conditional sampling through quadrant analysis [*Willmarth and Lu*, 1972] and their statistics have been investigated for a variety of flow and wall-roughness conditions (e.g., experiments in open-channel [*Nakagawa and Nezu*, 1977, NN77 hereafter], wind-tunnel [*Raupach*, 1981], stable [*Gao et al.*, 1989] and unstable [*Katul et al.*, 1997b] atmospheric boundary layers, and open-channel suspension flow [*Hurther and Lemmin*, 2003]). Besides the dominant role of the sweeps close to a rough wall, an "equilibrium region" is often, albeit not always [*Krogstad et al.*, 1992], observed in fully-developed turbulent flows in which the statistical properties of the two mechanisms are independent of the wall roughness over a significant portion of the flow. Direct relations established between the bursting events and the turbulent energy budget via turbulent diffusion [NN77] and a simple, but successful, structural turbulence model for triple products of velocity and scalar [*Nagano and Tagawa*, 1990] make the quadrant analysis an attractive tool.

Under-ice boundary layer [*McPhee and Morison*, 2001] is nearly always a zone of turbulent shear-flow between the ice and the underlying undisturbed ocean. Direct measurements of turbulent fluxes under drifting pack ice [e.g., *McPhee*, 1992; *McPhee and Martinson*, 1994] have provided a relatively comprehensive view of the associated turbulent processes, but as far as we know, conditional statistics for the Reynolds stress under drifting ice have not been previously examined. In this work we do so, in order to compare with existing theory and with other boundary layer studies. The extension of this work to scalar (salt and heat) turbulent fluxes is the topic for an ongoing companion paper and will be reported elsewhere.

Site and measurements

Under the Winter ARctic Polynya Study (WARPS), the German icebreaker *FS Polarstern* was moored to a large ice floe. During 1-2 April 2003, one vertical mast comprising two turbulent instrument clusters (TICs), nominally at 1 m and 5 m below the ice, was deployed from a hydrohole on pack ice drifting at an average speed of 15 cm s^{-1} in the Whaler's Bay, north of Svalbard. The site of deployment was chosen sufficiently away from the vessel on a relatively smooth, refrozen lead of 100 m x 50 m, and 110-cm thick ice,

surrounded by ~2-m thick ice dominated by ridges. Nearby conductivity-temperature-depth profiles showed a mixed layer thickness of ~30 m.

Each TIC comprises a Sontek acoustic current meter, a SeaBird Electronics (SBE) fast-response temperature sensor (SBE 03) and a ducted conductivity meter (SBE 04), all mounted to measure at the same vertical level at 2 Hz. The system is capable of resolving velocity and temperature fluctuations well into the inertial subrange and typical properties and data processing are described in detail elsewhere [e.g., *McPhee*, 1992; 1994]. Here we analyze velocity data from three runs of 345, 90, and 360 min length, separated by 18 and 258 min, between 1 April, 1223 UTC, and 2 April, 0614 UTC.

Quadrant analysis

The method and the related theory are summarized briefly for completeness (see NN77 for details). The longitudinal, u, and vertical, w, components of the velocity are aligned along x- and z-axes, with the wall (ice/ocean boundary) lying in the horizontal plane and positive z downward, such that the kinematic Reynolds shear stress $\tau = -\langle u'w' \rangle$ is the wallward flux of streamwise momentum. In the following the brackets and primes denote time averages and zero-mean fluctuations, respectively.

The quadrant-analysis is originally devised to sort contributions to τ from each quadrant of instantaneous values on the $u' - w'$ plane. Events from quadrant i are labeled as outward interactions (i=1; u'>0, w'>0), ejections (i=2; u'<0, w'>0), wallward interactions (i=3; u'<0, w'<0), and sweeps (i=4; u'>0, w'<0). Ejection and sweep events are the positive contributions to τ and transport the momentum excess outward and wallward, respectively. The contribution of quadrant i excluding a hyperbolic hole region of size $H = |u'w'|/|\langle u'w' \rangle|$ is defined as $\{u'w'\}_{i,H} = \langle u'w' I_{i,H} \rangle$, where curly brackets indicate conditional averages. The indicator function $I_{i,H} = 1$ when (u',w') is in quadrant i and larger than a fraction of the average flux set by H, and $I_{i,H} = 0$, otherwise. H = 0 corresponds to including all the events, and by progressively increasing H, larger events are detected. The threshold value of H to delineate large flux events is often chosen arbitrarily, typically when the contribution of interaction events ceases. The time fraction of associated contributions is $TF_{i,H} = \langle I_{i,H}(u',w') \rangle$. The stress fraction [*Raupach*, 1981] for quadrant i is defined by the flux contribution to $u'w'$ from the corresponding quadrant as $S_{i,H} = \{u'w'\}_{i,H}/\langle u'w' \rangle$. Because $\langle u'w' \rangle < 0$, $S_{1,H}$, $S_{3,H} < 0$ and $S_{2,H}$, $S_{4,H} > 0$, and for H = 0, $S_{1,0}+S_{2,0}+S_{3,0}+S_{4,0} = 1$.

NN77 derived the conditionally sampled probability density functions (pdf) of normalized Reynolds stress, $\omega = u'w'/\langle u'w' \rangle$, from a high-order cumulant discard Gram-Charlier pdf as

$$p_1(\omega) = p_G(\omega) + \psi^+(\omega); \ p_3(\omega) = p_G(\omega) - \psi^+(\omega); \ \omega < 0$$
$$p_2(\omega) = p_G(\omega) + \psi^-(\omega); \ p_4(\omega) = p_G(\omega) - \psi^-(\omega); \ \omega > 0 \tag{1}$$

where

$$p_G(\omega) = \frac{Re^{Rt}}{2\pi} \frac{K_0(|t|)}{(1-R^2)^{1/2}}, \quad S^\pm \equiv \frac{(S_u \pm S_w)}{2}, \quad D^\pm \equiv \frac{(D_u \pm D_w)}{2}$$

$$\psi^+(\omega) = \frac{Re^{Rt}}{2\pi} \frac{K_{1/2}(|t|)|t|^{1/2}}{(1-R)^2} \left[(1+R)\left(\frac{S^+}{3} + D^+\right)|t| - \left(\frac{2-R}{3}S^+ + D^+\right) \right] \tag{2}$$

$$\psi^-(\omega) = \frac{Re^{Rt}}{2\pi} \frac{K_{1/2}(t)t^{1/2}}{(1+R)^2} \left[(1-R)\left(\frac{S^-}{3} + D^-\right)t - \left(\frac{2+R}{3}S^- + D^-\right) \right]$$

Here, R is the negative of the correlation coefficient, K_x is the xth order modified Bessel function of the second kind, and $t \equiv R\omega/(1-R^2)$. S_u and S_w are the skewness of u' and w', respectively. D_u and D_w correspond to turbulent diffusion in the longitudinal and vertical directions. The non-conditional pdf of the normalized shear stress is $p(\omega) = 2p_G(\omega)$. If we denote the fluctuating velocity components rescaled by one standard deviation σ by circumflex (e.g., $\hat{u} = u'/\sigma_u$) by definition, $R = -\langle \hat{u}\hat{w} \rangle$, $S_u = \langle \hat{u}^3 \rangle$, $S_w = \langle \hat{w}^3 \rangle$, $D_u = \langle \hat{u}\hat{w}^2 \rangle$, and $D_w = \langle \hat{u}^2\hat{w} \rangle$.

Results and discussion

The data recovered from each TIC were divided into 15-min realizations, and the mean longitudinal velocity was aligned along the mean horizontal velocity direction, i.e., $\langle v \rangle = \langle w \rangle = 0$. Fluctuation time series were obtained by linearly detrending each segment. Over a total of 53, 42 segments were chosen when turbulence was fully-developed and the signal strength was well above the background noise with $\tau > 3.5 \times 10^{-5}$ m^{2}s^{-2}. As a result, $\sim 7.6 \times 10^4$ u'-w' pairs were analyzed from each TIC. On average, $|\langle v'w' \rangle|/|\langle u'w' \rangle| < 0.1$ at both levels and the flow can be considered two dimensional.

Ensemble-averaged quantities that describe the experiment are listed in Table 1. The correlation coefficient, -R, increases slightly with distance from the wall. The mean temperature at both levels is ~1°C above the freezing point referenced to the surface. Dissipation rate of turbulent kinetic energy (TKE) per unit mass, ε, and the vertical mixing length scale, λ, derived from the inertial subrange and the peak of the variance-preserving w′ spectra, respectively [*McPhee*, 1994], are not significantly different at the measurement depths. The friction velocity, $u_* = (\langle u'w'\rangle^2)^{1/4}$, hence τ, increases by 20% with distance from the interface, possibly because the flow adjusts to larger roughness elements over longer averaging path [*McPhee*, 1994]. This increase in u_* can play a significant role in the TKE balance [*McPhee*, 2004]. An order of magnitude estimate for the roughness length, derived from mean U/u_* at 5 m using law-of-the-wall, is $z_o \sim 0.2$ cm. Here U is the mean horizontal velocity. The associated roughness Reynolds number, $Re = u_* 30 z_o/\nu$ is 430 ± 100, using u_* derived from the uppermost TIC, and the viscosity $\nu = 1.4\times10^{-6}$ m^{2}s^{-1}, hence the flow is hydrodynamically rough. In terms of non-dimensional depth, in order to compare with the laboratory experiments, our uppermost TIC is at $z = 1$ m which is $z^+ = u_* z/\nu, \sim 7000$ wall distance away from the wall, or taking the depth of the flow as the mixed layer depth, $h\sim$ 30m, is at $z/h = 0.03$.

The fractional contributions to the Reynolds stress τ clearly show that the ejection and sweep events dominate over the interaction events (Figure 1), in accordance with the literature. Figure 1 can be interpreted as follows. At 1 m, the contributions from quadrants are $S_{1,0} = -0.46$, $S_{2,0} = 0.92$, $S_{3,0}=-0.43$, $S_{4,0}=0.97$, the sum of which is 1. Corresponding values at H=5 are, $S_{1,5} = -0.23$, $S_{2,5} = 0.53$, $S_{3,5}=-0.2$, $S_{4,5}=0.63$, the sum of which is 0.73, i.e. 73% of τ occurs in events more than 5 times the average τ, pointing the intermittent nature of the turbulence. The intensities of all events decrease with increasing distance from the wall.

The importance of the third and higher order moments as well as the relative intensity of sweep events at both levels is emphasized by the comparisons shown in Figure 2. Here $S_{i,H}$ is calculated by numerically integrating the composite average joint pdf of û-ŵ over a range of H. The joint Gaussian distributions are symmetric, hence theoretical curves for ejection and sweep contributions are the same. At 1 m, for about $H > 4$ the asymmetry between ejection and sweep contributions is apparent, whereas at 5m, the measured ejection-sweep stress fraction is not significantly different from correlated joint Gaussian within 90% confidence. This indicates that, at 5 m, the third and higher order moments are relatively less significant and function $\psi^-(\omega)$ in Eq. 2 is negligible. The difference $\Delta S_H = S_{4,H}-S_{2,H}$ between

the stress fractions due to sweeps and ejections is two times larger at 1 m than at 5 m for H ≤ 15. The value of this parameter at H = 0, i.e., ΔS_0, and the skewness S_u and S_w are reported to be approximately proportional [*Raupach*, 1981]. This has significant impact in understanding the behavior of the TKE flux, $F_{TKE} = \frac{1}{2} \langle w'(u'^2+v'^2+w'^2) \rangle$, which is related to ΔS_0 through $F_{TKE} = c_1 \Delta S_0 (c_2 \sigma_u^2 \sigma_w + c_3 \sigma_w^3)$ where c's are constants [*Raupach*, 1981]. The transport term in the TKE balance, $-\partial F_{TKE}/\partial z$, will yield local TKE loss when positive values of ΔS_0 (sweeps dominate) decrease with distance from the wall [*Raupach*, 1981]. The average values of ΔS_0 are 0.06 and 0.03 at 1 m and 5 m, respectively. This rate of decrease is comparable with the measured F_{TKE}/u_*^3 equal to -0.5 and -0.23 at 1 m and 5 m, respectively. Despite being inconclusive due to undersampling in vertical, this approximately linear correspondence between F_{TKE} and ΔS_0 indirectly suggests that σ_u and σ_w remain independent of depth at the measured z/h range, which is correct within 15% in our data set.

Assuming that contribution of S_u and S_w to ΔS_0 is negligible, *Katul et al.* [1997a] and *Poggi et al.* [2004] demonstrated that a truncated version of a third-order cumulant expansion model gives $\Delta S_0 \approx -(D_w-D_u)/2R(2\pi)^{1/2}$. Regression of measured ΔS_0 (84 ensembles) upon that modeled sets the slope to 0.99 and the intercept at 0.017 with the correlation coefficient of determinations 0.98 and a standard error of 0.04. We suggest that the truncated model is adequate to capture ΔS_0 from the measured R, D_u and D_w in the under-ice boundary layer. Combining this truncation with standard second order gradient-diffusion closure models for triple velocity moments [e.g., *Katul and Albertson*, 1998] yields

$$\Delta S_0 = \frac{-1}{2\sqrt{2\pi}} \frac{q\lambda_z}{\langle u'w' \rangle} \left[\frac{1}{\sigma_u} \frac{\partial \langle u'u' \rangle}{\partial z} - \frac{2}{\sigma_w} \frac{\partial \langle u'w' \rangle}{\partial z} \right] \qquad (3)$$

where $q^2 = 2 \times TKE$ and λ_z is a mixing length proportional to z (i.e., $\lambda_z = a\kappa z$ with $\kappa = 0.4$ and a = u_*/q). In order to reproduce $\Delta S_0 = 0.06$ at 1 m, a mixing length of $\lambda_z = 0.3$ m is required in Eq. 3 which is 2.5 times that obtained using the definition of λ_z with the measured a ≈ 0.29. We note that the mixing length inferred from spectral analysis (Table 1) is larger, however, above analysis can help to determine an equivalent length scale to retain the non-local effects of the ejection-sweep cycle under drifting ice for gradient-diffusion closure of the TKE transport term.

The time fraction for ejection and sweep are $TF_{2,0}$= 0.31 (0.3) and $TF_{4,0}$=0.29 (0.3) at 1 m (5m), respectively, and agree within 4% to those reported for open channel water [NN77], open channel oil [*Brodkey et al.*, 1974] and for atmospheric surface layer over tall-natural grass surface [*Katul et al.*, 1997b].

The ensemble-averaged pdf of the normalized Reynolds stress (Figure 3) agrees favorably with the theory, $p(\omega)=2p_G(\omega)$ calculated using R given in Table 1. The long tails of the $p(\omega)$ emphasize the intermittency as evidenced by Figure 1. We further calculated the conditional pdf from measurements and contrasted to that derived from Eqs. 1-2 (Figure 4). Particularly at 1 m, despite having a lower peak, sweep events have larger values for H > 8, suggesting a larger contribution to the Reynolds stress. The theoretical curves again represent the measurements reasonably well. Discrepancies at large H can be attributed to the limited (third) order moments implemented in the theory.

Subsequently we conclude that the non-conditional and the conditional u′w′-covariance statistics under drifting ice can be reasonably well represented by a second order pdf and a third order cumulant discard Gram-Charlier distribution, respectively, in agreement with earlier pioneering work [*Lu and Willmarth*, 1973; NN77]. At 5 m, the stress-fractions of ejection and sweep events are found to be nearly symmetrical and can be estimated fairly well by joint-Gaussian pdf. Clear dominance of ejection and sweep events over interaction events are observed. The difference in sweep-ejection stress fractions at 1 m is found to be twice as large as that at 5 m. Violent events at short time scales, with a considerable amount of the Reynolds stress might have consequences for the heat and salt fluxes, hence melting/freezing in the under-ice boundary layer, and the related turbulent transfer coefficients. The transported stress fractions are closely related to the third order moments of fluctuating velocity components and quadrant analysis might improve our understanding of the vertical transport of TKE, particularly in investigating the case (which is fairly common under sea ice and a fairly vast data set is available) where the stress increases with distance from the boundary. In this aspect there is similarity with turbulent flow within and above canopies [*Raupach and Thom*, 1981] where the elements of the canopy generate turbulent wakes at length scales characteristics of the canopy elements. The relations established for canopy flows are shown to capture the salient features resolved by our observations; however future work is merited to examine the TKE budget in the under-ice boundary layer.

References

Brodkey, R.S., J.M. Wallace, and H. Eckelmann, Some properties of truncated signals in bounded shear flows, *J. Fluid Mech.*, *63*, 209-224, 1974.

Cantwell, B.J., Organized motion in turbulent flow, *Annu. Rev. Fluid Mech.*, *13*, 457-515, 1981.

Gao, W., R.H. Shaw, and U.K.W. Paw, Observation of organized structure in turbulent flow within and above a forest canopy, *Boundary-Layer Meteorol.*, *59*, 35-57, 1989.

Hurther, D., and U. Lemmin, Turbulent particle flux and momentum flux statistics in suspension flow, *Water Resour. Res.*, *39*, 1139, doi:10.1029/2001WR001113, 2003.

Katul, G.G., and J.D. Albertson, An investigation of higher-order closure models for a forested canopy, *Boundary-Layer Meteorol.*, *89*, 47-74, 1998.

Katul, G.G., C.-I. Hsieh, G. Kuhn, D. Ellsworth, and D. Nie, Turbulent eddy motion at the forest-atmosphere interface, *J. Geophys. Res.*, 102, 13409-13421, 1997a.

Katul, G.G., G. Kuhn, J. Schieldge, and C.-I. Hsieh, The ejection-sweep character of scalar fluxes in the unstable surface layer, *Boundary-Layer Meteorol.*, *83*, 1-26, 1997b.

Krogstad, P.A., R.A. Antonia, and L.W.B. Browne, Comparison between rough- and smooth-wall turbulent boundary layer, *J. Fluid Mech.*, *245*, 599-617, 1992.

Lu, S.S., and W.W. Willmarth, Measurements of the structure of the Reynolds stress in a turbulent boundary layer, *J. Fluid Mech.*, *60*, 481-512, 1973.

McPhee, M.G., Turbulent heat flux in the upper ocean under sea ice, *J. Geophys. Res.*, *97*, 5365-5379, 1992.

McPhee, M.G., On the turbulent mixing length in the oceanic boundary layer, *J. Phys. Oceanogr.*, *24*, 2914-2031, 1994.

McPhee, M.G., A spectral technique for estimating turbulent stress, scalar flux magnitude, and eddy viscosity in the ocean boundary layer under pack ice, *J. Phys. Oceanogr., in press*, 2004.

McPhee, M.G., and D.G. Martinson, Turbulent mixing under drifting pack ice in the Weddell Sea, *Science*, *263*, 218-221, 1994.

McPhee, M.G., and J.H. Morison, Under-ice boundary layer, in *Encyclopedia of Ocean Sciences*, edited by J.H. Steele, S.A. Thorpe, and K.K. Turekian, pp. 3069-3076, Academic Press, 2001.

Nagano, Y., and M. Tagawa, A structural turbulence model for triple products of velocity and scalar, *J. Fluid Mech.*, *215*, 639-657, 1990.

Nakagawa, H., and I. Nezu, Prediction of the contributions to the Reynolds stress from bursting events in open-channel flows, *J. Fluid Mech.*, *80*, 99-128, 1977.

Poggi, D., G.G. Katul, and J.D. Albertson, Momentum transfer and turbulent kinetic energy budgets within a dense model canopy, *Boundary-Layer Meteorol.*, 111, 589-614, 2004.

Raupach, M.R., Conditional statistics of Reynolds stress in rough-wall and smooth-wall turbulent boundary layers, *J. Fluid Mech.*, *108*, 363-382, 1981.

Raupach, M.R., and A.S. Thom, Turbulence in and above plant canopies, *Annu. Rev. Fluid. Mech.*, 123, 97-129, 1981.

Robinson, S.K., Coherent motions in the turbulent boundary layer, *Annu. Rev. Fluid Mech.*, *23*, 601-639, 1991.

Willmarth, W.W., and S.S. Lu, Structure of the Reynolds stress near the wall, *J. Fluid Mech.*, *55*, 65-92, 1972.

Table 1. Mean values and standard deviations of the correlation coefficient, -R, the friction velocity, u_*, its ratio to the mean flow, U/u_*, temperature, θ, salinity, S, dissipation, ε, and vertical mixing length, λ, at 1 m and 5 m below the ice.

| TIC level (m)	1	5
R	0.27 ± 0.1	0.32 ± 0.09
u_* (cm s^{-1})	1 ± 0.25	1.2 ± 0.3
U/u$_*$	22 ± 7	20 ± 4
θ (°C)	-0.95 ± 0.05	-0.93 ± 0.06
S	34.44 ± 0.02	34.45 ± 0.02
ε (x10^{-6} W kg^{-1})	2.1 ± 1.4	2.3 ± 1.3
λ (m)	1.3 ± 0.8	1.7 ± 1.0
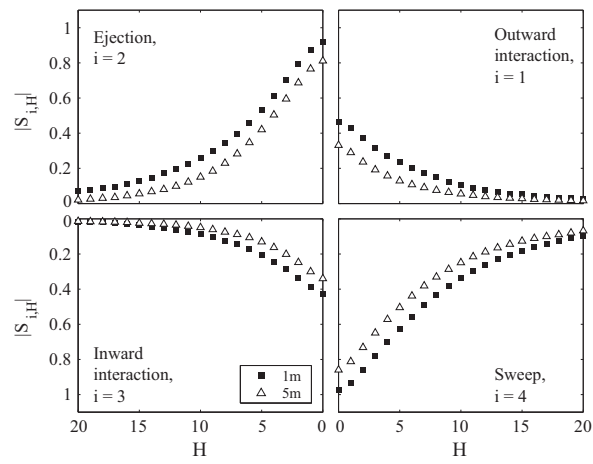
Figure 1. Fractional contributions to the Reynolds stress as a function of the hole size, H at 1 m and 5 m below the ice.
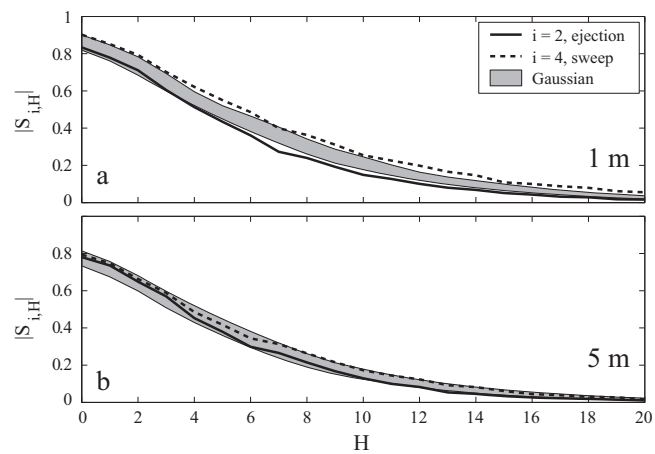
Figure 2. Ejection (solid) and sweep (dashed) magnitudes at (a) 1 m and (b) 5 m below the ice. The gray band envelopes the joint Gaussian pdf derived from 90% bounds on 999 bootstrapped samples of 42 u'-w' correlations.
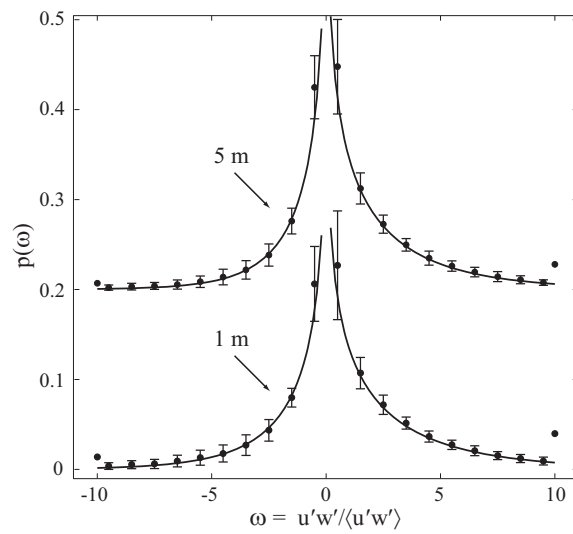
Figure 3. Theoretical and experimental pdf of the normalized Reynolds stress, ω at 1 m and 5 m (off-set by 0.2 in the ordinate) below the ice. Theoretical curves are $p(\omega)=2p_G(\omega)$. The experimental values and errorbars are the average and one standard deviation, respectively, over 42 ensembles. The sum of probability exceeding $\pm\omega=10$ are indicated.
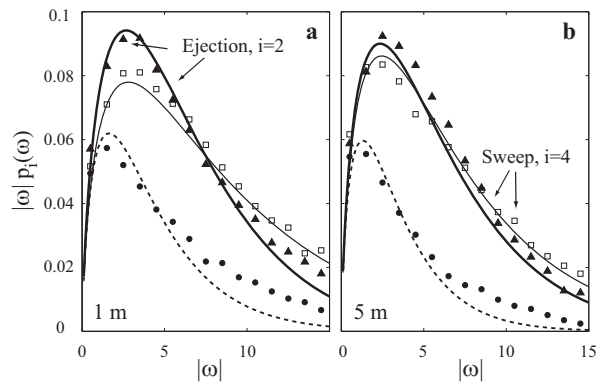
Figure 4. Conditional pdfs at 1-m and 5-m. The theoretical curves (thick, i=2; thin, i=4) are calculated from Eqs.1-2. Those for interaction events (i=1, 3) are indistinguishable, and their mean is plotted (dashed) for clarity. Observed values are shown by triangles for ejection, squares for sweeps, and dots for the average of interaction events.